4ICEGE
Thessaloniki-GREECE 2007

4th International Conference on
Earthquake Geotechnical Engineering
June 25-28, 2007
Paper No. 1335

INVESTIGATION ON SEISMIC BEHAVIOR OF A ROAD EMBANKMENT ON SOFT GROUND BASED ON EARTHQUAKE OBSERVATION RECORDS

Satoshi NISHIMOTO[1], Takaaki IKEDA[2], Noboru KAMIAKITO[3] and Shigeru MIWA[4]

ABSTRACT

In the city of Tomakomai, Hokkaido, the seismic behavior of soft ground and of a road embankment built on such ground have been observed, toward investigating the seismic performance of a road embankment constructed on soft ground and improving seismic engineering. Earthquake observations on soft ground started in 1991 at two locations, one where volcanic ash soil predominates and the other where sandy soil predominates. Observation records have been obtained for 17 earthquakes, including the Hokkaido Toho-Oki earthquake (M_j8.2), and they have been used to clarify the seismic behavior of soft ground, whose complexity makes its seismic behavior nonlinear. Earthquake observations started at a road embankment in 1996, and records have been obtained for 9 earthquakes whose maximum amplitudes ranged from less than 10 cm/s/s to the more than 100 cm/s/s of the 2003 Tokachi-Oki Earthquake (M_j8.0). This study uses these records to examine the nonlinear seismic behavior of a road embankment. The results show that the seismic behavior of soft ground and the road embankment is nonlinear, that a cross-sectional area of the embankment behaves as an integrated system, and that the low-order natural frequency is roughly the same in the ground as in the embankment.

Keywords: Road embankment, Soft ground, Nonlinearity, Earthquake observation, Seismic behavior

INTRODUCTION

Road infrastructure is required to be highly seismic performance, so as to ensure evacuation routes and transportation of emergency supplies after earthquakes. One road structure component is an embankment. It is often used in road structures because the construction cost is reasonable and surplus soil excavated in local construction projects can be used at the sites instead of being discarded. Because an embankment is built directly on the ground, its seismic behavior is greatly influenced by the seismic behavior of the ground. Thus, an embankment should be considered as a system coupled with the ground when its seismic performance is examined.

The Civil Engineering Research Institute for Cold Region has been conducting observations on the seismic behavior of soft ground and road embankments built on such ground, for the purpose of determining the seismic performance of such embankments and developing seismic engineering. At two locations on a foundation bed -- one where volcanic ash soil predominates and the other where

[1] Civil Engineering Research Institute for Cold Region, Public Works Research Institute, Japan, Email: nishimoto@ceri.go.jp
[2] Research Institute of Technology, Tobishima Corporation, Japan, Email: takaaki_ikeda@tobishima.co.jp
[3] Research Institute of Technology, Tobishima Corporation, Japan, Email: noboru_kamiakito@tobishima.co.jp
[4] Research Institute of Technology, Tobishima Corporation, Japan, Email: shigeru_miwa@tobishima.co.jp

sandy soil predominates -- seismic observations were done with vertical arrays and with liquefaction arrays in which piezometers were installed to record excess pore water pressure. The liquefaction array observation provides valuable records on earthquake-generated increases in excess pore water pressure (Hayashi et al., 2000, Nishikawa et al., 2001, Nishikawa et al., 2002).

Ground observations during the 2003 Tokachi-Oki Earthquake, in which the maximum acceleration exceeded 100 cm/s/s, and other low- and medium-intensity earthquakes have been recorded. The observations revealed that when the maximum acceleration acting on the embankment is great, the nonlinear amplification characteristics of the ground become more prominent and the increase in excess pore water pressure accelerates (Nishimoto et al., 2006). The seismic observations of a road embankment started in 1996, and records for 9 earthquakes have been obtained. Thus, data have been accumulated from low strong-motion intensities to high strong-motion intensities -- high enough to cause non-linear behavior of the ground.

Based on the above, this paper uses observations records obtained at a road embankment and soft ground in and after 1996 to examine the seismic behavior of the embankment overlying such ground, particularly from the viewpoint of its nonlinear seismic behavior.

SEISMIC OBSERVATIONS

Observation sites

The seismic observation sites are southwest of Lake Utonai, in the northeastern part of Tomakomai. Fig. 1 shows the sites. The observation sites are in the southern part of a lowland belt 40 ~ 60 km north-south, extending from Ishikari to Tomakomai in the Yufutsu Plain. Fig. 2 shows a longitudinal geologic profile from northwest to southeast. On the northwest side of the figure lies a tableland of Shikotsu volcanic ash. The northwestern half of the area in the figure is largely secondary sediments of volcanic ash and pumice originating in the tableland. The southeastern half includes distributions of beach sand and viscous soil from the back swamp (Committee for Publication of Regional Geology of Japan, 1993, Soya and Sato, 1980).

The ground observations were done at Site A and Site B, which are predominantly distributed with volcanic ash and sandy soil, respectively. The two sites are about 1.4 km apart. Figs. 3(a) and 3(b) show soil profiles. The ground at Site A mainly consists of secondary sediment of volcanic ash.

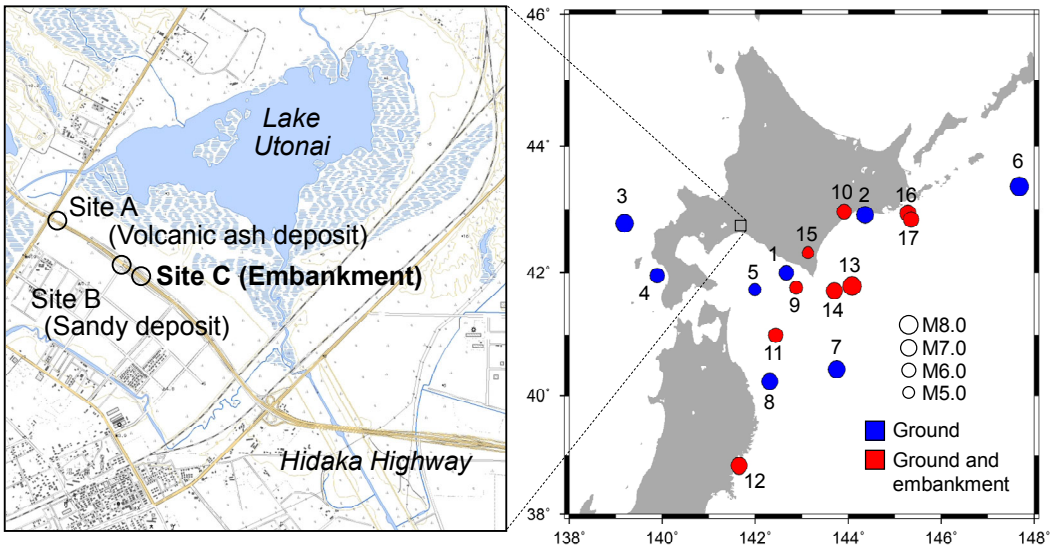

Figure 1. Location of investigation site and epicenters of earthquakes

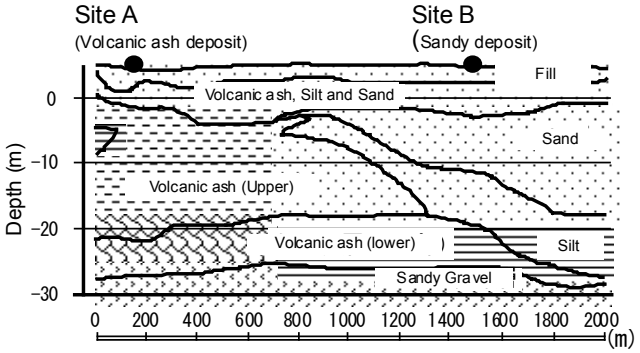

Figure 2. Cross section observation sites (left: N-W; right: S-E)

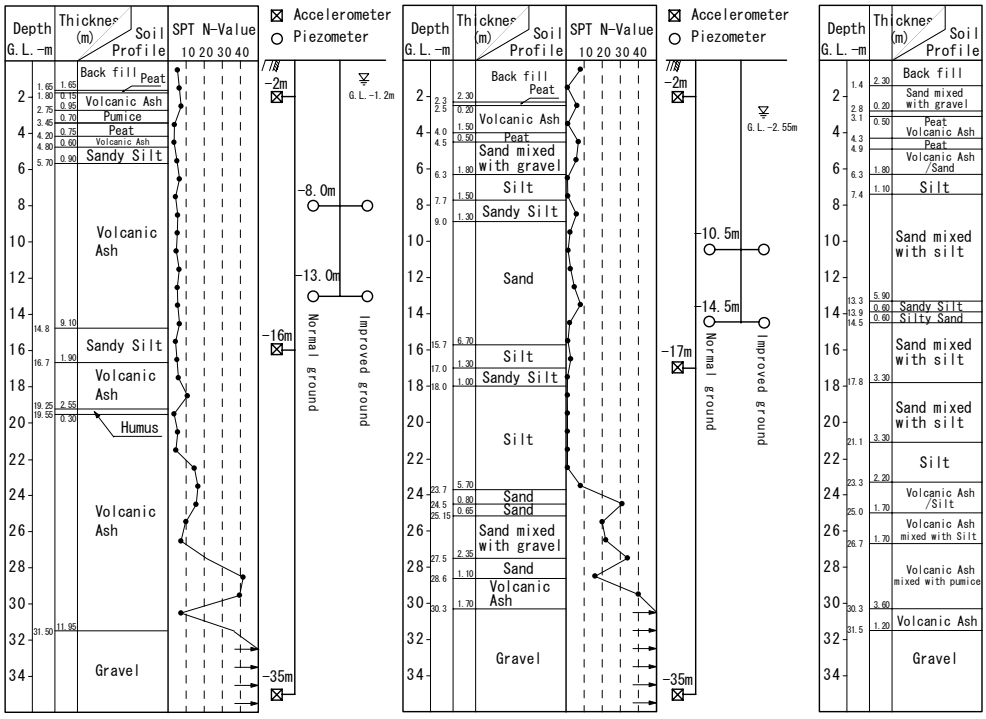

(a)Site A (b)Site B (c)Site C

Figure 3. Soil profile and instrumentation

Volcanic ash and sandy silt are loosely deposited from G.L. –6 m to –20 m. These layers have *N*-values of 5 or less, indicating that they are easily liquefiable. At Site B, there are layers of volcanic ash, peat and silt alternate to the depth of G.L. –9 m, and a loose sandy layer extends from G.L. –9 m to –16 m. The liquefaction potential is high for the loose sand layer there. While the composition of the subsurface layers differs between Site A and Site B, as shown in Fig. 2 and Fig. 3, it is presumed that the subsurface layers at both sites lie on the same gravel bed.

The embankment observation site (Site C) is 50 m east of Site B. Fig. 3(c) shows a profile of the soil at Site C. There are layers of sandy soil, peat and silt alternate to the depth of G.L. –7 m, which overlie a layer of sandy soil extending to the depth of G.L. –20 m. The gravel bed, which is presumed to be the engineering foundation basis, is at G.L. – 31 m. Although the ground strength at Site C is unknown because *N*-values are not known, the composition of the subsurface layers at Site C is similar to that at Site B; thus, the seismic behavior of ground at Site C is approximated by the seismic behavior at Site B.

Earthquake observation system

Fig. 3 shows a soil profile of Sites A and B, including the installation depths of the accelerometers and piezometers. Accelerometers were installed at three different depths in the unimproved ground (without liquefaction countermeasures.) At both Site A and Site B, the deepest installation point is G.L. –35 m in the gravel layer where the S-wave velocity exceeds 400 m/s. The gravel layer is widely distributed in this area. The accelerometers installed at the shallowest point (G.L. –2 m) and the deepest point measure 2 horizontal components and 1 vertical component, whereas that installed between them measures only 2 horizontal components.

Four piezometers were installed within the liquefiable layers: two in the improved ground (i.e., that in which liquefaction countermeasures had been taken) at different depths and two in unimproved ground at different depths. The purpose was to determine the effectiveness of the ground improvements.

Fig. 4 shows the embankment profile, including the accelerometers. The embankment is 7.35 m high and has a crest length of 25.0 m. As shown in the Fig. 3, volcanic ash and sandy soil have high potential for liquefaction at the time of an earthquake. As a liquefaction countermeasure, ground improvement by the installation of sand compaction piles (SCPs) 15 m wide and 15 m deep has been applied on both sides of the embankment. The accelerometers were installed at the top of the slope (Point A), at the center of the crest (Point B) and at the base of the embankment (Point C.) At each of these three points, the observations consist of 2 horizontal components and 1 vertical component. Because the ground behavior of the embankment can be approximated by the behavior of sandy ground (Site B) as mentioned above, the accelerometers in the embankment are synchronized with those in the sandy ground.

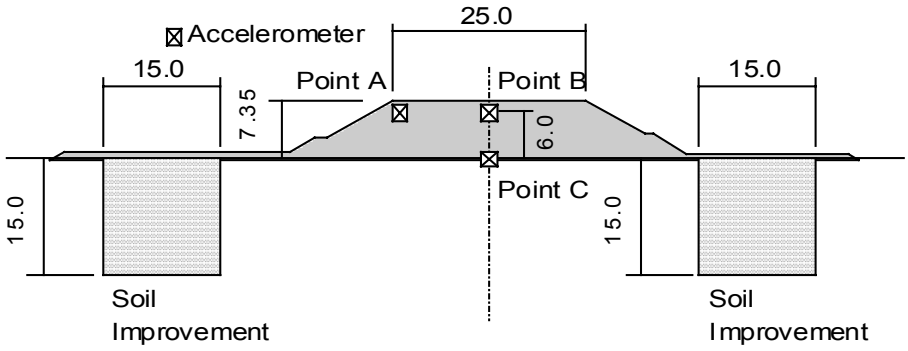

Figure 4. Embankment profile, with instrumentation

SUMMARY OF SEISMIC OBSERVATIONS

Seismic data

Table 1 shows the earthquake data observed since the start of seismic observations in 1991. Observation at Site C started in 1996; records prior to then are not available. Additionally, because observations at Site B are synchronized with those at Site C but not with those at Site A, not all of the earthquakes were recorded at all three sites. At Site C, records for 9 earthquakes were obtained. That with the greatest intensity was the 2003 Tokachi-Oki Earthquake (M_j8.0), and the 8 others include 3 earthquakes with magnitudes of 6 and 3 with magnitudes of 7. The epicenters are shown in Fig. 1 (Japan Meteorological Agency, 2005).

Observation records

Table 1 shows the maximum horizontal acceleration. In this table, the ground observation records are converted into values in the axial direction of the embankment and the direction transverse to that. Errors caused by the mis-orientation of the seismometer at Point B of Site C were corrected. The

maximum velocity was calculated as follows: First, baseline correction was done using the mean values for the initial 5 seconds of the motions in the time history of acceleration. Then, after applying a 0.1-Hz high-pass filter, the Fourier integral was used to obtain waveforms of the velocity time history, which were used to calculate the maximum velocity. Regarding the years after 1996, when the seismic observations of the embankment started, the largest acceleration was recorded at the time of the 2003 Tokachi-Oki Earthquake. Because records at the depth of G.L. –2 m were not obtained in earthquake 10 (Eq10), the strong motion records for the 8 other earthquakes are used in this study.

Table 1. Profiles of earthquakes and observed records

No	Earthquake				Maximum acceleration (cm/s/s)															
					Free Field (Upper : Site A , Bottom : Site B)								Embankment							
	Region	Mj	Location	Depth	G.L.-2m			G.L.-17m			G.L.-35m		Point A			Point B			Point C		
	Date-Time			(km)	AX	TR	UD	AX	TR	AX	TR	UD	AX	TR	UD	AX	TR	UD	AX	TR	UD
Eq01	Uraga-Oki	6.3	41°59.8'	64	10.7	13.7	4.4	8.8	8.5	6.8	8.0	3.9	-	-	-	-	-	-	-	-	-
	1991.11.27 04:40:48.9		142°39.9'		17.0	15.9	8.3	12.4	10.9	9.6	7.6	3.3									
Eq02	Kushiro-Oki	7.5	42°55.0'	101	-	-	-	-	-	-	-	-	-	-	-	-	-	-	-	-	-
	1993.01.15 20:06:07.2		144°21.4'		127.8	94.7	46.7	75.5	69.4	74.0	50.6	25.0									
Eq03	Hokkaido-Nanseioki	7.8	42°46.8'	35	13.0	15.8	6.1	10.6	12.5	8.6	10.9	4.6	-	-	-	-	-	-	-	-	-
	1993.07.12 22:17:11.7		139°11.0'		14.5	21.8	6.8	13.7	15.9	10.8	13.8	5.3									
Eq04	Hokkaido-Nanseioki	6.3	41°57.3'	24	6.0	11.2	2.5	4.1	6.0	3.5	4.2	2.3	-	-	-	-	-	-	-	-	-
	1993.08.08 04:42:43.6		139°53.1'		5.9	13.7	2.7	4.4	7.7	2.9	5.1	2.1									
Eq05	Tomakomai-Oki	5.4	41°43.4'	80	13.7	10.8	8.0	7.3	8.2	5.7	5.5	2.8	-	-	-	-	-	-	-	-	-
	1993.12.04 18:30:14.2		141°59.3'		*	*	5.1	8.5	8.8	10.3	8.7	2.5									
Eq06	Hokkaido-Touhouoki	8.2	43°22.3'	28	47.2	47.1	24.8	22.7	29.2	19.8	20.9	11.2	-	-	-	-	-	-	-	-	-
	1994.10.04 22:22:56.9		147°40.7'		83.6	86.7	36.3	40.9	46.7	*	*	15.9									
Eq07	Sanrikuharuka-Oki	7.6	40°25.6'	0	44.8	79.7	10.0	31.7	38.5	24.6	25.9	7.7	-	-	-	-	-	-	-	-	-
	1994.12.28 21:19:20.9		143°44.9'		53.8	74.7	15.4	32.2	35.9	*	*	7.7									
Eq08	Iwateken-Oki	7.2	40°13.2'	48	18.7	23.3	4.9	9.4	12.5	8.3	11.3	3.8	-	-	-	-	-	-	-	-	-
	1995.01.07 07:37:37.1		142°18.5'		*	*	6.0	12.5	11.4	*	*	3.5									
Eq09	Urakawa-Oki	5.9	41°45.4'	49	-	-	-	-	-	-	-	-	6.1	7.2	4.8	6.2	7.1	4.7	4.7	5.1	2.8
	1997.02.20 16:55:00.3		142°52.5'		5.3	6.7	3.0	3.5	5.4	3.3	2.9	1.5									
Eq10	Kushiro-Shicho-Nanbu	6.3	42°57.9'	106	12.7	15.7	5.0	8.2	8.3	4.8	4.2	3.0	21.9	19.0	8.4	22.3	18.8	7.3	19.2	17.2	5.6
	1999.05.13 02:59:23.1		143°54.5'		*	*	5.5	11.3	10.4	8.6	6.1	3.3									
Eq11	Aomoriken-Touhouoki	6.4	40°59.5'	38	10.0	12.5	6.0	8.2	6.6	4.6	5.0	2.4	21.4	15.2	5.3	21.3	14.2	5.7	16.0	12.6	4.6
	2001.08.14 05:11:24.9		142°26.4'		22.1	13.7	6.8	12.8	9.3	10.5	5.6	2.6									
Eq12	Miyagiken-Oki	7.1	38°49.0'	72	8.7	11.5	3.8	5.2	8.4	5.6	6.4	1.9	14.9	14.6	4.1	14.6	13.5	3.7	13.5	12.8	3.0
	2003.05.26 18:24:33.4		141°39.2'		15.9	13.1	3.4	9.4	8.7	6.1	6.3	2.3									
Eq13	Tokachi-Oki	8.0	41°46.7'	42	94.2	83.0	29.8	85.0	59.6	74.0	56.9	25.0	124.2	131.1	64.8	120.7	137.6	61.7	112.2	127.3	44.0
	2003.09.26 04:50:07.6		144°4.7'		127.0	132.4	53.6	74.4	79.2	69.7	76.0	25.7									
Eq14	Tokachi-Oki	7.1	41°42.4'	21	41.0	40.0	18.2	27.6	25.7	23.2	20.9	12.2	62.5	57.7	46.8	51.0	52.3	34.9	42.9	41.8	23.0
	2003.09.26 06:08:01.8		143°41.7'		57.9	49.0	31.6	41.8	39.3	29.0	25.8	15.5									
Eq15	Tokachi-Shicho-Nanbu	5.2	42°19.1'	48	-	-	-	-	-	-	-	-	19.7	16.8	8.8	16.2	14.1	6.5	9.6	9.8	4.4
	2004.06.11 03:12:10.1		143°080'		15.5	11.8	5.9	9.5	9.7	7.5	6.6	2.0									
Eq16	Kushiro-Oki	7.1	42°566'	48	12.8	22.7	4.7	9.0	11.5	8.4	7.0	4.1	15.8	23.2	7.7	15.8	22.4	7.8	15.0	21.2	7.1
	2004.11.29 03:32:14.5		145°167'		15.2	21.7	6.6	11.5	11.5	8.4	13.8	3.7									
Eq17	Kushiro-Oki	6.9	42°507'	46	14.3	11.3	4.4	9.1	7.5	6.8	5.4	4.1	20.3	19.9	5.3	19.9	19.4	5.8	19.4	17.5	5.4
	2004.12.06 23:15:11.8		145°208'		19.3	18.1	4.8	15.1	12.9	10.3	6.8	3.4									

SEISMIC BEHAVIOR OF THE EMBANKMENT

Cross-sectional behavior

Regarding the embankment and the ground, Table 1 shows the maximum accelerations transverse to the embankment. Fig. 5 shows distributions of maximum accelerations in the depth direction in the embankment and the ground. The maximum accelerations in the embankment are shown by white circles, and those in the ground are shown by white squares. The maximum accelerations at Point A are shown by black circles to distinguish them from those at Point B, which is at the same height in the embankment. The maximum acceleration in the embankment and that in the ground are amplified relative to that at G.L. –35 m, which is the engineering foundation basis. The maximum accelerations at G.L. –2 m are equal to or greater than those at Point C (G.L. ±0 m), which is at roughly the same depth as G.L. –2 m. This difference in maximum acceleration may be attributed to the difference in seismic observation sites. But it is also possible that the embankment base is subject to restraint by the mass of the embankment, which restrains the seismic behavior at the base. Fig. 6 shows depth distributions of the maximum velocities. The maximum velocity and the maximum acceleration are amplified in the embankment and in the ground. But the amplification is smaller than that of the maximum acceleration except in Eq15.

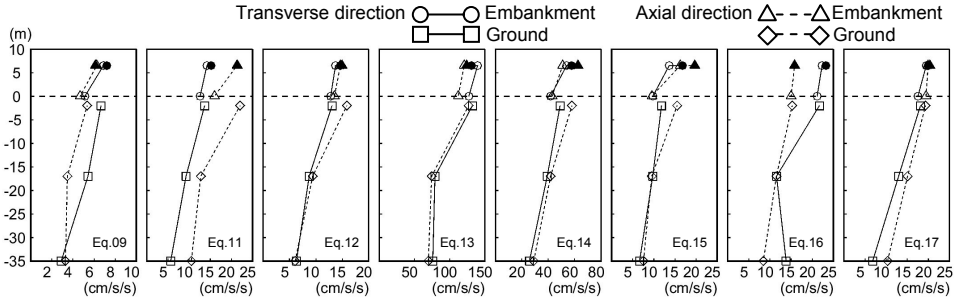

Figure 5. Distribution of maximum acceleration

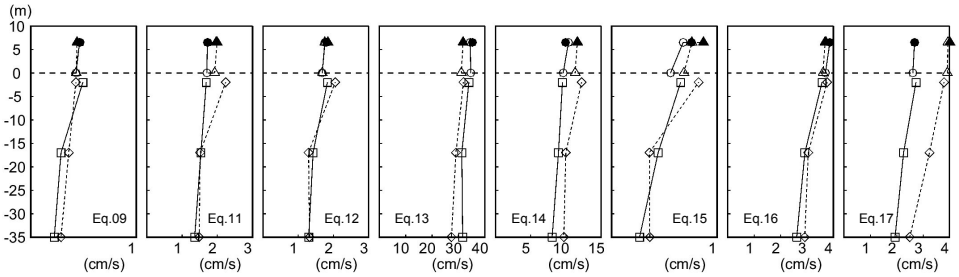

Figure 6. Distribution of maximum velocity (transverse to embankment axis)

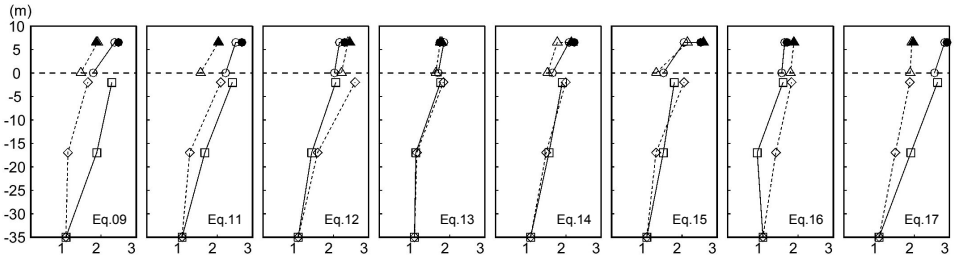

Figure 7. Distribution of maximum acceleration ratio (/G.L.-35m)

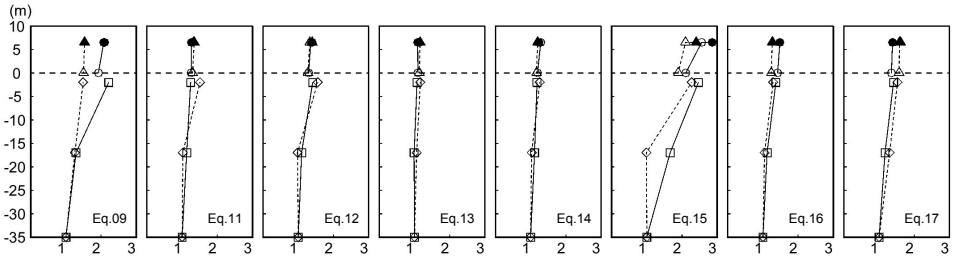

Figure 8. Distribution of maximum velocity ratio (/G.L.-35m)

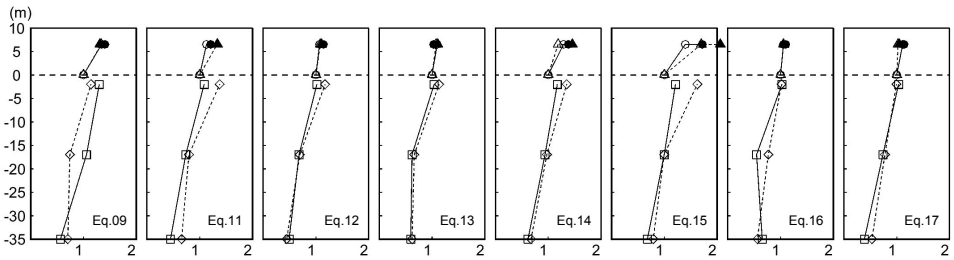

Figure 9. Distribution of maximum acceleration ratio (/Point C)

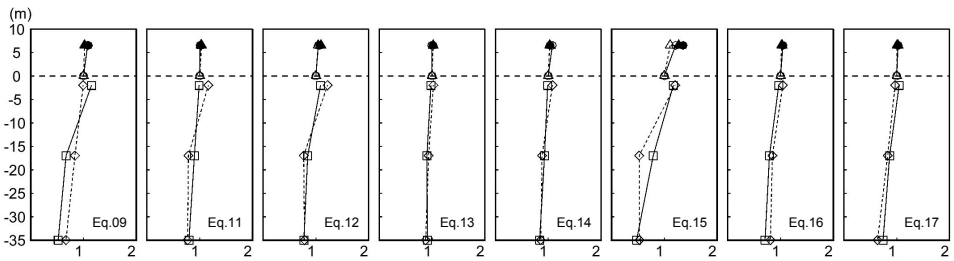

Figure 10. Distribution of maximum velocity ratio (/Point C)

Fig. 7 shows the depth distributions of maximum acceleration ratios (i.e., ratio of amplified maximum acceleration to maximum acceleration) normalized by the maximum value at G.L. –35 m. Fig. 8 shows the depth distributions of maximum velocity ratios (i.e., ratio of amplified maximum velocity to maximum velocity) normalized by the maximum value at G.L. –35 m. The maximum acceleration ratio represents the degree of amplification of the maximum acceleration, and the maximum velocity ratio represents the degree of amplification of the maximum velocity. The maximum acceleration ratios at G.L. –35 m differ for each earthquake. They are in the range of 1.68~2.93 at Point A and 1.62~2.86 at Point B. The maximum acceleration is amplified about 1.7 times at the both points. The maximum velocity ratios are in the range of 1.12~2.86 at Point A and 1.12~2.55 at Point B. Thus, both the maximum acceleration and the maximum velocity are amplified by roughly the same degree. However, if we exclude Eq09 and Eq15, whose maximum velocity at G.L. –35 m is small and whose maximum velocity ratio is large, then the maximum velocity ratio is 1.46 at Point A and 1.48 at Point B. Therefore, it can be said that the maximum velocity ratio is smaller than the maximum acceleration ratio.

Fig. 9 shows the depth distributions of maximum acceleration ratio normalized by the maximum acceleration at Point C. Fig. 10 shows the depth distribution of the maximum velocity ratio normalized by the maximum velocity at Point C. The maximum acceleration ratio and the maximum velocity ratio at G.L. –35 m represent the degree of amplification in the embankment and in the ground when they are considered to be an integrated system. The maximum acceleration ratio and the maximum velocity ratio at Point C represent the degrees of amplification in the embankment alone. The maximum acceleration ratios are in the range of 1.03~1.72 at Point A and 1.06~1.45 at Point B. Excluding Eq09 and Eq15, the ratios are 1.03~1.38 at Point A and 1.06~1.25 at Point B. The maximum velocity ratios, excluding Eq09 and Eq15, are 1.02~1.08 at Point A and 1.02~1.06 at Point B. Thus, the degree of amplification in the embankment alone is smaller than that in the embankment and the ground considered as an integrated system.

Fig. 11 shows transfer functions (Point A/Point C, Point B/Point C) of the embankment in Eq09, in which the maximum acceleration at Point C is small, and in Eq13, in which it is large. The transfer functions are smoothed by Parzen Window with a bandwidth of 0.2 Hz. In Eq09 and Eq13, the transfer functions at Point A and Point B are almost identical both in the transverse and axial directions of the embankment, and thus the seismic behavior at Point A and Point B are approximately the same. This suggests that local deformation did not occur in the embankment. However, the transfer functions in Eq09 and Eq13 differ greatly in form; thus, the response characteristics of the embankment seem to differ between Eq09 and Eq13.

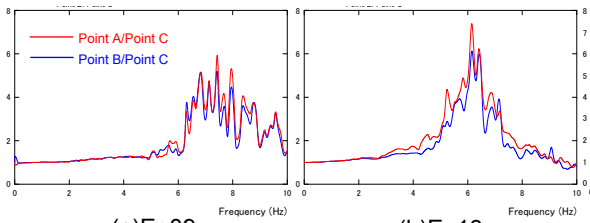

Figure 11. Transfer function of embankment (transverse to embankment axis)

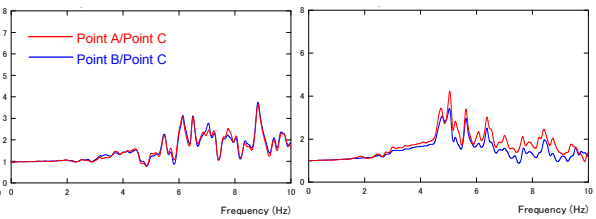

Figure 12. Transfer function of embankment (axial)

Behavior in the axial direction

For the embankment and the ground, Table 1 shows the maximum accelerations in the axial direction. Fig. 5 and Fig. 6 respectively show depth distributions of maximum acceleration and maximum velocity for strong motion in the axial direction. White triangles and white diamonds indicate the values for the embankment and for the ground, respectively. In Eq12, Eq14 and Eq15, but not Eq13, the maximum accelerations for strong motion in the axial direction of the embankment at G.L. –35 m are roughly the same as those in the transverse direction. In these three earthquakes, the maximum

accelerations at Point C in the axial direction are also roughly the same as those in the transverse direction. The degree of amplification of maximum velocity in the axial direction is smaller than that of the maximum acceleration in the axial direction, as was true for the transverse direction.

Fig. 7 shows the depth distributions of maximum acceleration ratios (i.e., ratio of amplified maximum acceleration to maximum acceleration) normalized by the maximum value at G.L. –35 m. Fig. 8 shows the depth distributions of maximum velocity ratios (i.e., ratio of amplified maximum velocity to maximum velocity) normalized by the maximum value at G.L. –35 m. Fig. 9 shows the depth distribution of maximum acceleration ratio normalized by the maximum value of acceleration at Point C. Fig. 10 shows the depth distribution of the maximum velocity ratio normalized by the maximum value of velocity at Point C. As shown in Fig. 9 and Fig. 10, the maximum response values in the transverse direction and the axial direction of the embankment are almost identical. In some earthquakes, the maximum response values in the ground differ between the transverse direction and the axial direction. Particularly in Eq09 and Eq15, in which the maximum response values are smaller than in the other earthquakes, they differ greatly between the two directions.

Fig. 12 shows the transfer functions in the embankment (Point A/Pont C, Point B/Point C) for Eq09 and Eq13. The transfer functions at Point A and Point B in the axial direction are almost identical to each other, as was true for the transverse direction. But comparison between Fig. 11 and Fig. 12 indicates that the transfer functions differ between the transverse direction and the axial direction in each of the earthquakes. This suggests that the frequency response characteristics differ between the two directions.

Behavior of the horizontal surface of the embankment

Regarding the embankment and the ground at G.L. –2 m and G.L. –35 m in Eq09, whose strong motion was of low intensity and Eq13, whose strong motions were of high intensity, Fig. 13 shows the particle motions of displacement at the horizontal surface. The vertical and horizontal axes show the axial and transverse directions of the embankment, respectively. Fig. 13 shows motions during a 30-second period that includes the principal shock.

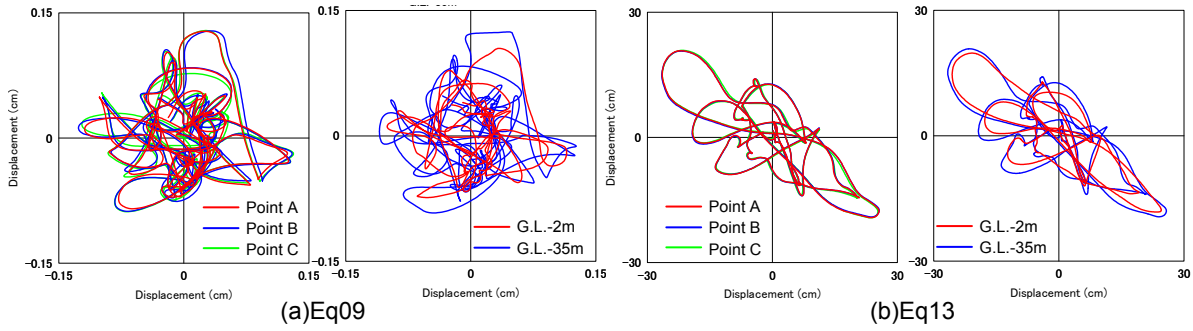

Figure 13. Horizontal displacement particle motion

In both Eq09 and Eq13, almost the same motion of displacement is found at Point A, Point B and Point C of the embankment. Thus the seismic behavior on the horizontal surface is identical at the three points. The particle motion of displacement in Eq09 shows no directionality, but there is a clear directionality of displacement for Eq13, with the orientation of the particle motion deviating 45 degrees from the embankment axis. Comparison between the particle motions of displacement in the embankment and that in the ground shows that they differ in the displacement amplitude but are similar in shape. This suggests that the seismic behavior in the embankment and the ground were the same.

ESTIMATION OF THE NONLINEAR BEHAVUOR OF THE EMBANKMENT

Strong motions and the maximum response values

Regarding the transverse direction of the embankment, the relationship between the maximum strong motion acting on the embankment and the maximum response value is examined below.

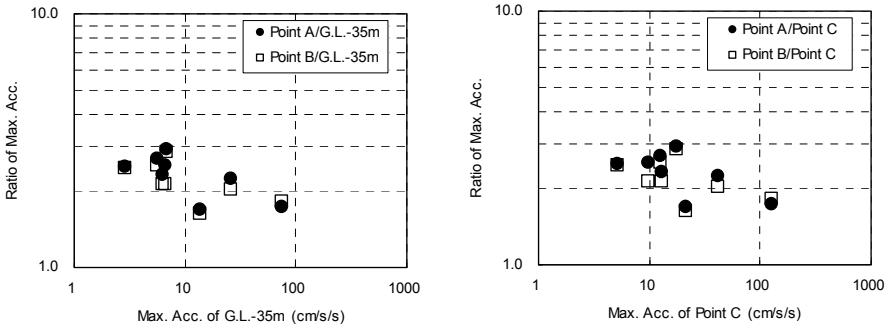

Figure 14. Relationship between ratio of maximum acceleration and maximum acceleration into the ground-embankment system (transverse to embankment axis)

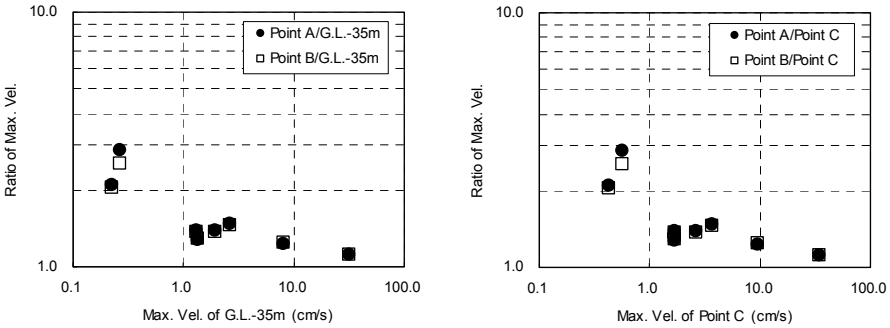

Figure 15. Relationship between ratio of maximum velocity and maximum velocity into the ground-embankment system (transverse to embankment axis)

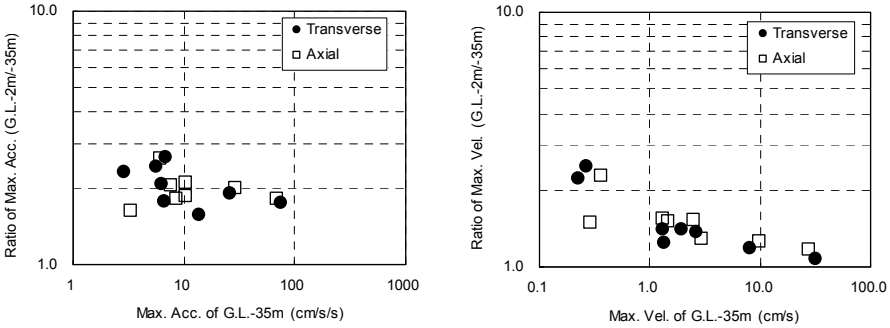

Figure 16. Relationship between ratio of maximum response and maximum input motion into the ground-embankment system

Fig. 14 (left) shows the maximum acceleration at G.L. –35 m, and the maximum acceleration ratios in the embankment (Points A and B) after normalization by the maximum acceleration at G.L. –35 m. Fig. 14 (right) shows the maximum acceleration at Points C, and the maximum acceleration ratios in the embankment (Points A and B) after being normalization by the maximum acceleration at Point C. In both cases, when the maximum acceleration acting on the embankment is great, the maximum acceleration ratio is low. Fig. 15 shows the results for maximum velocity. As in the case with the maximum acceleration above, when the maximum velocity acting on the embankment is great, the maximum velocity ratio is low. The maximum velocity ratio shows a particularly great change at the maximum input velocity of 1.0 cm/s for the case of normalization by the maximum value at G.L. –35 m and for the case of normalization by the maximum value at Point C. To clarify the behavior of the

ground, Fig. 16 shows the maximum acceleration ratio and the maximum velocity ratio at G.L. –2 m, both normalized by the maximum acceleration and the maximum velocity at G.L. –35 m. As was seen for the embankment, the degree of amplification is small when the intensity of strong motion is high.

Motion transfer characteristics of the embankment

In Fig. 17, the transfer functions in the transverse and axial directions are shown with regard to Point B at G.L. –35 m. The frequency range from 0 Hz to 10 Hz in this figure contains four peaks. Among the peak frequencies in the transverse and axial directions of the embankment, the third peak is slightly lower in the transverse direction than the three other peaks in three of the eight figures, but the first and the second peaks are almost identical to each other.

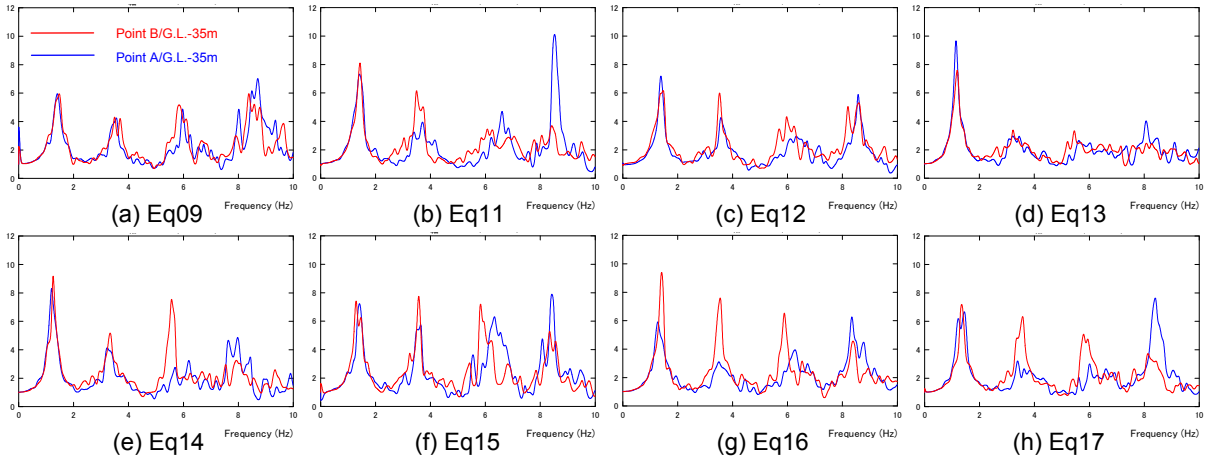

Figure 17. Transfer functions (transverse to embankment axis; Point A/G.L.-35m, Point B/G.L.-35m)

Fig. 18 shows the relationship between the maximum accelerations and the peak frequencies at G.L. –35 m and Point C. When the maximum acceleration is great, the absolute value of the peak frequency is small. In the transverse direction, the first and second peak frequencies at the greatest recorded maximum accelerations (Tokachi-Oki Earthquake) are 0.81 times 0.90 times, respectively, that for the smallest recorded maximum acceleration. In the axial direction, they are 0.79 times and 0.87 times, respectively, that for the smallest recorded maximum acceleration. On the assumption that the initial vibration is the predominant one in an integrated ground-embankment system and on the basis of the ratio of reduction of the first peak frequency, Equation (1) is used to estimate the reduction rate of the shear modulus in the ground-embankment system at the time of strong motion (Nishikawa et al., 2002). Where G^* is ratio of reduction in shear modulus at the time of a strong earthquake, Gs and Gw are shear modulus at the time of a strong earthquake and a weak earthquake respectively and fs and fw are first peak frequency at that time. The shear modulus is estimated to be reduced by a factor of 0.6~0.7.

$$G^* = \frac{Gs}{Gw} = \left(\frac{fs}{fw}\right)^2 \tag{1}$$

Fig. 19 compares the transfer functions at G.L. –2 m and G.L. –35 m. The transfer function in the ground is similar to that in the ground-embankment system, and the low-order peak frequencies are similar between the two. This suggests that the low-order vibration mode represents the vibration mode of the ground. Fig. 20 shows the transfer function in the center of the embankment in comparison with that at the base of the embankment. This transfer function can be taken as the transfer function in the embankment alone. Unlike in the transfer function at G.L. –35 m, only one or two distinctive peaks are found. Additionally, the transfer function in the transverse direction differs from that in the axial direction. On the other hand, the transfer function also shows a tendency for the peak frequency to be small when the maximum acceleration is great at the base of the embankment. The highest frequency is 7.1 Hz (in Eq11) and the lowest frequency is 6.1 Hz (in Eq13), making the

factor of reduction 0.85. When Equation (1) is used, the factor of reduction in shear modulus of the embankment is estimated to be 0.72.

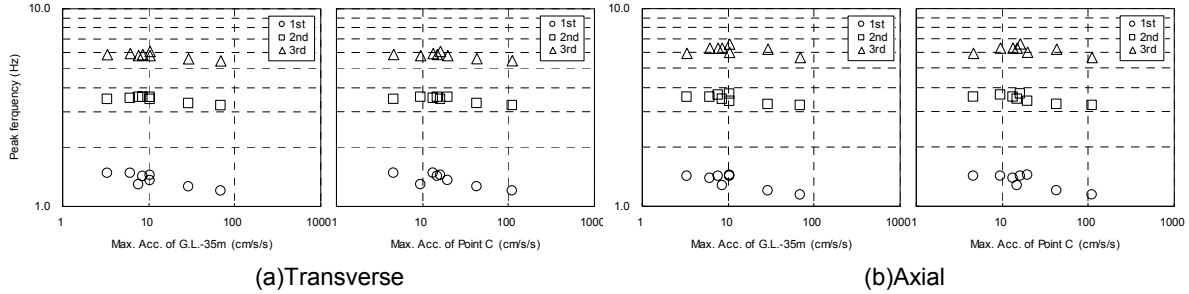

Figure 18. Relationship between peak frequency of transfer and maximum acceleration at G.L.-35m and at Point C

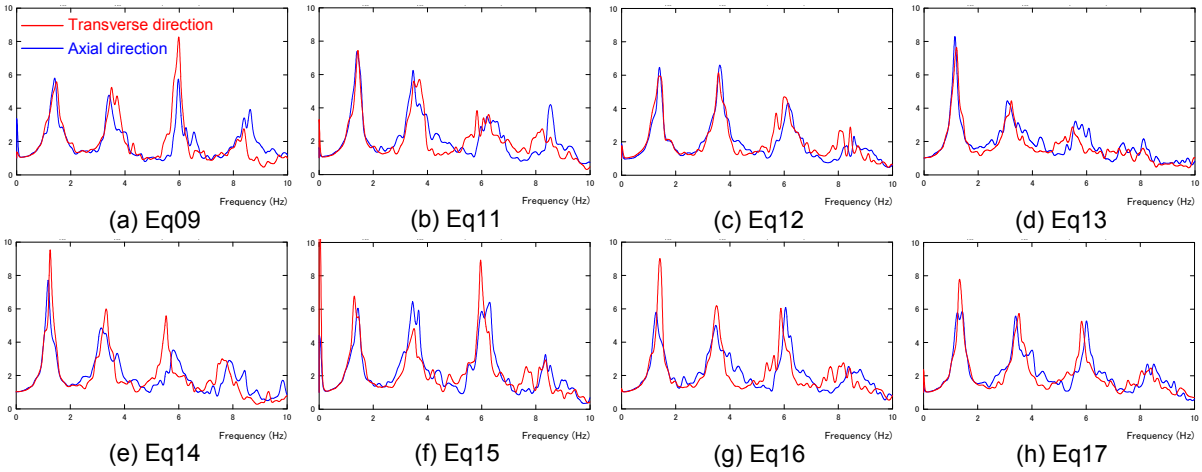

Figure 19. Comparison of transfer function (G.L.-2m/G.L.-35m) of transverse and axial directions

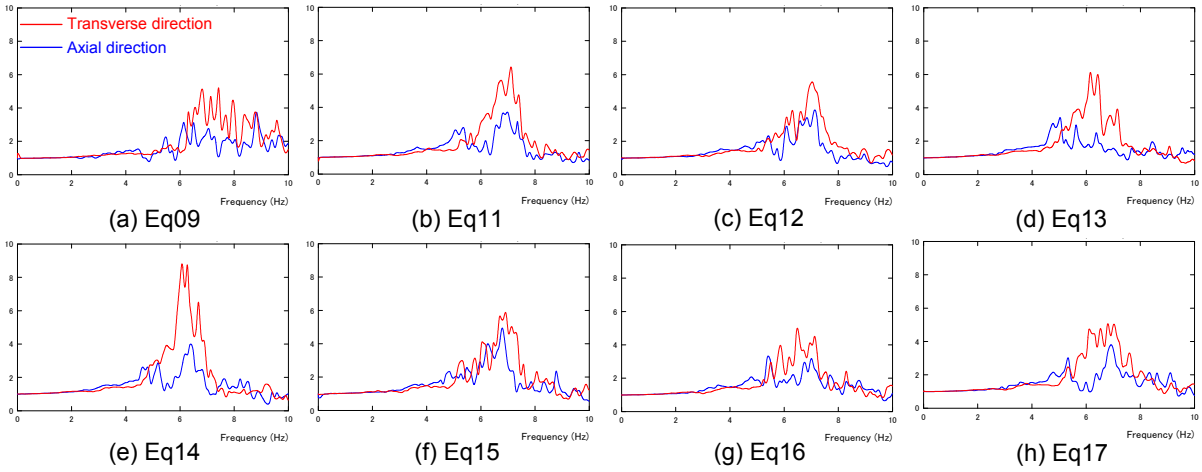

Figure 20. Comparison of transfer function (Point B/ Point C) of transverse and axial directions

CONCLUSIONS

Seismic observations were conducted in soft ground and in a road embankment built on such ground. The observation records were used to examine the seismic behaviors of the road embankment on soft ground, and the following results were obtained.

1) Records of strong motions in the embankment were obtained for 9 earthquakes. The maximum accelerations were found to range from less than 10 cm/s/s to more than 120 cm/s/s.
2) In the transverse direction of the embankment and soft ground, the degree of amplification for maximum acceleration was in the range of 1.6~2.9 and for maximum velocity it was in the range of 1.1~1.5. The maximum acceleration showed greater amplification than the maximum velocity. The amplification ratio in the embankment alone was 1.1~1.4 for the maximum acceleration and 1.0~1.1 for the maximum velocity, indicating that amplification in the embankment is smaller than that in the embankment and soft ground considered as an integrated system. The amplification in the axial direction, in terms of both the maximum acceleration and the maximum velocity, is almost the same as in the transverse direction.
3) The transfer function at the center of the crest is about the same as that at the top of slope of the embankment, and the particle motion of displacement on the horizontal surface is the same at these two points. This suggests that the ground and the embankment behave integrally without local deformation. However, because the transfer function in the transverse direction differs from that in the axial direction, the frequency response characteristics differ between the two directions.
4) When strong motion acting on the embankment is intense, the amplification of the embankment is small. This means that the amplification of the embankment is nonlinear. The amplification of the maximum velocity shows a sharp decrease at of 1.0 cm/s.
5) The transfer function of the soft ground and embankment system shows four distinctive peaks. The transfer function of the embankment alone has only one peak.
6) The peak frequency of the transfer function is low when strong motion intensity is high. On the assumption that the first-order mode was predominant in the embankment coupled with soft ground and in light of the ratio of reduction in the first peak frequency, it is presumed that the shear modulus in the ground-embankment system at the time of a strong earthquake was reduced by a factor of 0.6~0.7. For the embankment alone, the factor of reduction in shear modulus is estimated to be 0.7.
7) The transfer function of the soft ground and embankment system is similar to that of the ground alone, and both have similar frequencies at low-order peaks. This suggests that the low-order vibration mode represents the vibration mode of the ground.

REFERENCES

Committee for Publication of Regional Geology of Japan, Regional Geology of Japan Part 1 Hokkaido, *Kyoritsu Shuppan CO., LTD*., 1993. (in Japanese)

Hayashi,H., Nishikawa,J., Egawa,T., Miwa,S. and Ikeda,T., "Ground Seismic Behavior from Liquefaction Array Observation," *Proceedings of the 12th World Conference on Earthquake Engineering*, No.517, 2000

Japan Meteorological Agency, Earthquake Information, http:www.jma.go.jp/jma/indexe.html

Nishikawa,J., Hayashi,H., Egawa,T., Miwa,S. and Ikeda,T., "Evaluation of the Seismic Behavior on Sandy Ground with Built-up Pore Water Pressures by Effective Stress Analysis," *Proceedings of the 4th International Conference on Recent Advances in Geotechnical Earthquake Engineering and Soil Dynamics*, paper No.3.29, 2001.

Nishikawa,J., Hayashi,H., Egawa,T., Miwa,S. Ikeda,T. and Mori,S., "Liquefaction Array Observations at Two Sites and Analysis of their Records," *Journals of JSCE*, No.703/I-59, pp.327-343, 2002. (in Japanese)

Nishimoto,S., Miwa,S. and Ikeda,T., "Strong Motion of Records at the Tomakomai Liquefaction Array during the 2003 Tokachi-Oki Earthquake," *Proceedings of the First European Conference on Earthquake Engineering and Seismology*, paper No. 471, 2006.

Soya,T. and Sato,H., Geology of the Chitose District (1980), Geological Survey of Japan, 1980. (in Japanese)